HHS Public Access

Author manuscript

Neuroimage. Author manuscript; available in PMC 2025 May 16.

Published in final edited form as:

Neuroimage. 2024 September ; 298: 120764. doi:10.1016/j.neuroimage.2024.120764.

Age dictates brain functional connectivity and axonal integrity following repetitive mild traumatic brain injuries in mice

Marangelie Criado-Marrero[a,b,c,1], **Sakthivel Ravi**[a,b,c,1], **Ekta Bhaskar**[b,h], **Daylin Barroso**[a,b,c], **Michael A. Pizzi**[b,c,g,f], **Lakiesha Williams**[i], **Cheryl L. Wellington**[j], **Marcelo Febo**[c,d,e], **Jose Francisco Abisambra**[a,b,c,e,f,*]

[a]Center for Translational Research in Neurodegenerative Disease (CTRND), University of Florida, Gainesville, FL 32610, USA

[b]Department of Neuroscience, University of Florida, Gainesville, FL 32610, USA

[c]McKnight Brain Institute, University of Florida, Gainesville, FL 32610, USA

[d]Department of Psychiatry, University of Florida, Gainesville, FL 32610, USA

[e]Fixel Institute for Neurological Diseases, University of Florida, Gainesville, FL 32610, USA

[f]Brain Injury Rehabilitation and Neuroresilience (BRAIN) Center University of Florida, Gainesville, FL 32610, USA

[g]Department of Neurology, University of Florida, Gainesville, FL 32610, USA

[h]Department of Computer of Information Science and Engineering (CISE), University of Florida, Gainesville, FL 32610, USA

[i]J. Crayton Pruitt Family Department of Biomedical Engineering, Gainesville, FL 32610, USA

*Corresponding author: j.abisambra@ufl.edu (J.F. Abisambra).

[1]These authors contributed equally to this work.

Credit authorship contribution statement

Marangelie Criado-Marrero: Writing – review & editing, Writing – original draft, Visualization, Validation, Supervision, Project administration, Methodology, Investigation, Funding acquisition, Formal analysis, Conceptualization. **Sakthivel Ravi:** Writing – review & editing, Data curation, Conceptualization, Methodology, Investigation. **Ekta Bhaskar:** Writing – review & editing, Formal analysis. **Daylin Barroso:** Methodology, Investigation, Data curation. **Michael A. Pizzi:** Writing – review & editing. **Lakiesha Williams:** Writing – review & editing. **Cheryl L. Wellington:** Writing – review & editing, Writing – review & editing, Resources. **Marcelo Febo:** Writing – review & editing, Resources, Methodology. **Jose Francisco Abisambra:** Writing – review & editing, Validation, Supervision, Resources, Project administration, Funding acquisition, Conceptualization.

Declaration of competing interest

The authors declare no conflict of interest.

Data and code availability statement

We are dedicated to the broad and open dissemination of our research outcomes. In line with this, we will adhere to the NIH Grant Policy on Sharing of Unique Research Resources, which involves the Principles and Guidelines for Recipients of NIH Research Grants and Contracts on Obtaining and Disseminating Biomedical Research Resources (1999). Our data is securely stored in our institutional network computers and HiPerGator supercomputer. Access to data will be made possible after publication, in agreement with the policies established by the University of Florida. The corresponding author will be the contact to access and grant permission to transfer files. If any intellectual property necessitates a patent, we will ensure that the technology, materials, and data are accessible to the broader research community in accordance with the NIH Principles and Guidelines document.

Supplementary materials

Supplementary material associated with this article can be found, in the online version, at doi:10.1016/j.neuroimage.2024.120764.

[j]Department of Pathology and Laboratory Medicine, Djavad Mowafaghian Center for Brain Health, University of British Columbia, Vancouver, BC, V6T 1Z3, Canada

Abstract

Traumatic brain injuries (TBI) present a major public health challenge, demanding an in-depth understanding of age-specific symptoms and risk factors. Aging not only significantly influences brain function and plasticity but also elevates the risk of hospitalizations and death following TBIs. Repetitive mild TBIs (rmTBI) compound these issues, resulting in cumulative and long-term brain damage in the brain. In this study, we investigate the impact of age on brain network changes and white matter properties following rmTBI by employing a multi-modal approach that integrates resting-state functional magnetic resonance imaging (rsfMRI), graph theory analysis, diffusion tensor imaging (DTI), and neurite orientation dispersion and density imaging (NODDI). Our hypothesis is that the effects of rmTBI are worsened in aged animals, with this group showing more pronounced alterations in brain connectivity and white matter structure. Utilizing the closed-head impact model of engineered rotational acceleration (CHIMERA) model, we conducted rmTBIs or sham (control) procedures on young (2.5–3-months-old) and aged (22-months-old) male and female mice to model high-risk groups. Functional and structural imaging unveiled age-related reductions in communication efficiency between brain regions, while injuries induced opposhigh-risking effects on the small-world index across age groups, influencing network segregation. Functional connectivity analysis also identified alterations in 79 out of 148 brain regions by age, treatment (sham vs. rmTBI), or their interaction. Injuries exerted pronounced effects on sensory integration areas, including insular and motor cortices. Age-related disruptions in white matter integrity were observed, indicating alterations in various diffusion directions (mean diffusivity, radial diffusivity, axial diffusivity, and fractional anisotropy) and density neurite properties (dispersion index, intracellular and isotropic volume fraction). Neuroinflammation, assessed through Iba-1 and GFAP markers, correlated with higher dispersion in the optic tract, suggesting a neuroinflammatory response in injured aged animals compared to sham aged. These findings offer insight into the interplay between age, injuries, and brain connectivity, shedding light on the long-term consequences of rmTBI.

Keywords

Repetitive mild TBI; Diffusion tensor imaging; CHIMERA; Microglia; Resting state functional MRI; Aging

1. Introduction

Traumatic brain injuries (TBI) profoundly impact the global population affecting lifestyle and work productivity of an estimated 50 million individuals worldwide (Guan et al., 2023). They are a leading cause of disability imposing high economic burden of health costs for the individual and healthcare systems (Pavlov et al., 2019; Centers for Disease Control and Prevention, 2023). Among TBIs, repeated mild traumatic brain injuries (rmTBIs) are prevalent and underdiagnosed traumas (Centers for Disease Control and Prevention, 2023). Given the mild nature of these injuries and cofounding symptoms with other diseases, symptoms may not be noticeable shortly after the incident, which presents substantial

challenges to differentiate temporary effects and identify profound pathogenic signatures in brain (Centers for Disease Control and Prevention, 2023; Powell et al., 2008).

Repetitive mTBIs are a major risk factor for developing post-traumatic stress disorder (PTSD) and neurodegenerative conditions such as Alzheimer's disease and related dementias (ADRD) (Luo et al., 2023; Smolen et al., 2023; Mohamed et al., 2021; Abisambra and Scheff, 2014). Aging is a significant factor contributing to the elevated risk of these disorders and the occurrence of traumatic brain injury-related cases and fatalities (Gardner et al., 2018; Hou et al., 2019). However, whether aging and rmTBI, alone or in combination amplify brain dysfunction remains largely undefined. Exploring the intricate interplay between aging and rmTBI in relation to neurodegenerative conditions holds significant importance and warrants prompt attention to mitigate the risk posed by these factors.

Resting-state functional magnetic resonance imaging (rsfMRI) and diffusion tensor imaging (DTI) are valuable non-invasive tools used to define imaging biomarkers of brain damage after injury (Woodrow et al., 2023; Gugger et al., 2023; Palacios et al., 2017; D'Souza et al., 2020; Khong et al., 2016; Xu et al., 2021; Sakthivel et al., 2023). rsfMRI enables the evaluation of functional connectivity, whereas DTI captures structural alterations in the white matter fiber tracks. Combined with graph theory, these imaging techniques determine changes in topological brain networks and subnetworks, functional connections between regions of interest, morphology following rmTBI (Khong et al., 2016; Li et al., 2022; Kim et al., 2022; Moreira da Silva et al., 2020), and rmTBI associations with cognitive decline and neurodegeneration (Sakthivel et al., 2023; Coelho et al., 2021). Young and aged adults show a higher prevalence for TBI cases and deaths, as reported by Center of Disease Control (CDC) (Centers for Disease Control and Prevention, 2023). Notably, in aged adults, there is a delayed onset of symptoms, reduction of brain functions, and outcomes worsen after mTBI challenging evaluation of damage within the first days (Garza et al., 2020; Nyberg et al., 2010). This delayed response has been noticed in aged mice as well by manifesting prolonged brain edema resolution, slower axonal remyelination and extending inflammatory responses (Timaru-Kast et al., 2012; Onyszchuk et al., 2008; Sandhir et al., 2008). The suitability of assessing brain injury severity with the Glasgow Coma Score has been debated when used in elderly patients. This is due to the influence of medications and age-related decline in brain processes, which may disconnect the assessment from expected recovery or mortality rates (Garza et al., 2020; Livingston et al., 2005; Salottolo et al., 2014).

To thoroughly investigate age-related brain changes after rmTBI, we utilized rsfMRI and graph theory to delineate distinct connectivity patterns in the brains of young (2.5–3-months-old) and aged (22-months-old) mice, modeling higher-risk age groups similar to young adults and the elderly. This analysis was conducted within a standardized mouse common coordinate framework (CCFv3 atlas) and focused on 148 specific brain regions. Additionally, we assessed white matter integrity and its compartments by employing DTI and neurite orientation dispersion and density imaging (NODDI) techniques. Our hypothesis is that the effects of rmTBI are exacerbated in aged animals, with this group exhibiting more pronounced alterations in brain connectivity and white matter structure. This study represents an important step in characterizing age-related differences in connectivity during the initial days after rmTBI. These results form a basis for understanding network effects

in relation to age and injury. Long-term, we aim to translate these results for more effective diagnosis, brain activity monitoring, recovery prediction, and assessment of elderly patients with rmTBI.

2. Methods

2.1. Animal husbandry

We obtained C57BL/6J wild-type young mice of both sexes from Jackson Laboratory (Bar Harbor, ME, USA). The aged wild-type mice, originally from Jackson Laboratory, were provided by Dr. David R. Borchelt at the University of Florida. Young and aged animals were housed and maintained in the same room under a 12-hour light cycle in standard conditions with free access to water and food. All animal procedures were approved by the University of Florida's Institutional Animal Care and Use Committee and adhered to the guidelines outlined in the National Institutes of Health Guide for the Care and Use of Laboratory Animals.

2.2. Closed-head impact model of engineered rotational acceleration (CHIMERA)

We used CHIMERA to induce rmTBI following previously published protocols (Sakthivel et al., 2023; Namjoshi et al., 2014; Namjoshi et al., 2017). Male ($n = 22$) and female ($n = 10$) mice were randomly assigned to either sham or CHIMERA injury procedures at their respective age groups: 'young' at 2.5–3 months [Sham, $n = 8$; rmTBI, $n = 10$] and 'aged' at 22 months old [Sham, $n = 6$; rmTBI, $n = 8$] (Fig. 1A). Control and injured mice received isoflurane (maintained at 1–2.5 %). The mouse's head is fixed in a supine position with a cushioned hole, minimizing rebound impact and delivering the impact into the dorsal cortical region. The injured group received two mild closed-head impacts with an energy level of 0.6 joules occurring 24 h apart; the sham group did not sustain impacts. Mice were injected subcutaneously with meloxicam (10 mg/kg) to control pain within 48 h. Tissue collection was performed at either 7 days (young) or 26 days (aged) after injury. This study only includes tissue examination in the aged group. Immunohistochemistry results for gliosis and other disease-like markers in young mice were reported previously (Sakthivel et al., 2023).

2.3. Loss of righting reflex (LRR) and weight records

Animals were weighed before the injury or sham procedures. The loss of righting reflex (LRR) is an innate behavior in animals, indicating their inclination to return to an upright position from a supine one. Following the impact, each mouse was placed on its back to measure the LRR, representing the duration taken to regain an upright position. LRR is considered analogous to the role of loss of consciousness duration in humans (Berman et al., 2023).

2.4. Imaging procedures

2.4.1. Image collection: Anatomical (T2), diffusion-weighted, and functional (fMRI) images were collected from animals at five days post-injury. Consistent with our previous protocol, animals were anesthetized with isoflurane (4 % for initiation and 1 % during maintenance) and medical-grade air (70 % N_2: 30 % O_2) to minimize stress and facilitate

high-quality image acquisition (Sakthivel et al., 2023). Image scanning was completed at the Advanced Magnetic Resonance Imaging and Spectroscopy Facility at the University of Florida in Gainesville, FL using a 11.1T MRI scanner (Magnex Scientific Ltd, Oxford, UK). Each animal was positioned to minimize motion artifacts under a radiofrequency coil tuned to 470.7 MHz (1 H resonance). This coil generated electromagnetic fields to detect nuclear magnetic resonance signals. A T2-weighted TurboRARE sequence was used with parameters: TE (echo time) = 41.42 msec, TR (repetition time) = 4000 msec, RARE factor = 16, average number = 12, FOV (field of view) 15 mm × 15 mm, 0.9 mm slice thickness, and a data matrix of 256 × 256 with 14 interleaved ascending coronal slices. Resting-state fMRI were acquired via a single-shot spin echo (SE) echo planar image (EPI) blip-up and blip-down sequence with parameters: TE = 15 msec, TR = 2000 msec, 600 repetitions, and a data matrix of 64 × 48 with 14 interleaved ascending coronal slices in the same space as the reference scan (anatomical).

For diffusion, image acquisition was completed in four shot 2-shell SE-EPI using the following parameters: TE = 19 msec, TR = 4000 msec, average number = 4, gradient duration = 3 msec, diffusion time spacing = 8 msec, FOV = 11 mm x 0.11 mm, slice thickness = 0.7 mm, matrix = 128 × 96, slice per mouse = 17. For DTI analysis, 47 images were collected, a B0 baseline image and 46 images with gradient directions for b values of 600 and 2000 s/mm^2.

2.4.2. Image preparation: The University of Florida HiPerGator supercomputer was used to complete all image processing. Images were converted from Bruker to NifTI format. All rsfMRI images underwent a comprehensive pre-processing pipeline using Analysis of Functional NeuroImages (AFNI) (Cox, 1996), Functional MRI of the Brain Library (FSL) (Smith et al., 2004), Advanced Normalization Tools (ANTs) software as outlined previously (Sakthivel et al., 2023). Pre-processing involved distortion and phase correction using FSL's TOPUP, removal of time series spikes and slow temporal variations, noise decomposition applying the independent component analysis (ICA), removal of skull using three-dimensional pulsed coupled neural networks (PCNN3D) in MATLAB (Fig. 1B). Manual correction of image masks was performed using ITK-SNAP (Yushkevich et al., 2006). Additional processing steps involved spatial smoothing (0.4 mm), and extraction of time series data. Time series from functional images, divided into 600 vol, were linearly aligned (using FSL FLIRT) and nonlinearly transformed (using ANTS) to the anatomical image. Then, these were aligned and registered to the two times down sampled parcellated mouse common coordinate framework (version 3, or CCFv3) (Wang et al., 2020) which was used as template to determine coordinates corresponding to 148 regions of interest (ROI) across the brain (Supplemental Table 1).

2.4.3. Network metrics in rsfMRI: Timeseries correlations among ROIs were calculated by Pearson's coefficient resulting in 10,878 relationships per brain. Fisher transformation was applied to normalize correlation coefficients before running analyses. The Brain Connectivity toolbox in MATLAB identified complex network properties and regional interactions. Network analysis was calculated using established methodologies (Sakthivel et al., 2023; Pompilus et al., 2020). Edge density thresholds ranging from

2 % to 40 % were systematically applied to evaluate a spectrum of global network metrics capturing strongest connections. Network strength measures the overall connectivity computed as the sum of edge weights connected to a region (node) indicating strength of communication between these connections. The characteristic path length measures the efficiency of information transfer, capturing how readily information spreads across the network. Global efficiency quantifies the brain's overall ability to integrate information across distant regions. The small-world index (SWI) represents a balance between local clustering and global efficiency, offering a more detailed understanding of network topology. For ROI-specific measures, a uniform 10 % threshold was used as this edge density may provide a comprehensive view of both strong and moderate connections in the brain network. BrainNet Viewer was used to illustrate brain connectome maps (Xia et al., 2013).

2.4.4. Diffusion tensor imaging (DTI) and neurite orientation dispersion and density imaging (NODDI): Bruker diffusion-weighted images were converted to NifTI files and then small and large shells were combined into one image using fslmerge. Images with severe noise (exhibiting high interference, random fluctuations in the signal, abnormal motion distortions) were excluded from the study. The remaining images were converted to mif files for Mrtrix software processing (Tournier et al., 2019). Denoising (enhancing signal-to-noise ratio), Gibbs ringing (suppressing artifactual oscillations), phase encoding (correcting for motion distortions), B1 field inhomogeneity (mitigating variations in the RF field) were applied to the data (Fig. 1C). These steps ensure higher accuracy and uniform signals across the brain before analysis.

For DTI, FSL's dtifit and CAMINO were used for linear and nonlinear diffusion tensor model application into our diffusion-weighted data computing fractional anisotropy (FA; values from 0 to 1), mean diffusivity (MD; in mm^2/s), radial diffusivity (RD; in mm^2/s), and axial diffusivity (AD; in mm^2/s). For NODDI, 54 vol composed of B0 (total of 2), b value of 600 s/mm^2 (total of 6), and b value of 2000 s/mm^2 (total of 46) images were processed adapting published protocols (Colon-Perez et al., 2019). To characterize microstructural properties, the orientation dispersion (OD), intra-cellular volume fraction (ICVF), and isotropic volume fraction (ISOVF) were calculated in neural tissues using NODDI AMICO software package (Daducci et al., 2015). Preprocessed DTI and NODDI images were then aligned to the mouse CCFv3 reference atlas. We first applied linear and nonlinear registrations between FA images, which has the best resolution among the DTI scans, to the reference atlas. The resulting linear transformations in FA were applied to the MD, RD, AD, OD, ISOVF, and ICVF images. After all images were aligned to a standard space, a common mask was applied to exclude any extra borderlines in images. Guided by atlas parcellations, manual segmentations were drawn for 36 ROIs in a common group template using ITK-SNAP (Supplemental Table 2). A single value corresponding to mean voxel intensity was extracted per region of interest (ROI) using the FSL fslstats function.

2.5. Immunohistochemical analysis

Ionized calcium-binding adapter molecule 1 (Iba-1) and glial fibrillary acidic protein (GFAP) staining was performed as previously established (Sakthivel et al., 2023). In brief, 5 μm coronal brain sections underwent deparaffinization, rehydration, and antigen retrieval.

Endogenous peroxidase was eliminated using the mixture of 0.3 % H_2O_2 in phosphate-buffered saline (PBS) and 10 % Triton X-100 (100 μl for 200 ml), and sections were blocked with 10 % goat serum. Tissue was incubated overnight with anti-Iba-1 (1:1000, PA5–27,436, Invitrogen) and anti-GFAP (GA5) (1:1000, CS3670S, Cell Signaling) antibodies followed by 30 min incubation with biotinylated secondary antibodies. Sections were then treated with an avidin-biotin complex reagent and developed in DAB (Cat# 5510–0031). Image quantification used Image Scope software (v12.4.3.5008) with positive pixel count program. Average values from three sections per brain determined Iba-1 and GFAP expression.

2.6. Statistical analysis

Network and tissue analyses were conducted using GraphPad Prism software (version 10.0.3). Global network outcomes were described using repeated measures two-way ANOVA, correcting for multiple comparisons with the Tukey test. All statistical analyses for the imaging data were performed using R (v4.1.2). Before running analyses, data were assessed for normal distribution and homogeneity of variances between the groups. Extreme outliers were identified using the interquartile range method. Main effects of age (young vs. aged) and injury (sham vs. rmTBI) were tested by type III two-way ANOVA on each ROI with false discovery rate Benjamini-Hochberg (5 % FDR-BH) correction. ROIs resulting in statistically significant (p value<0.05) by main effects were followed by post-hoc analyses. Significant differences between group pairs were accounted when pairwise comparisons with FDR-BH shown $p < 0.05$ together with a large Cohen's effect size (+/− 0.8) between comparing means. A two-way ANOVA with Tukey HSD correction was used for weight and LRR measures. Two-tail unpaired Welch's t-test were used for glial analyses.

3. Results

3.1. Experimental design and global network properties

We investigated the extent to which age and rmTBIs influence behavior, overall brain network stability and white matter properties. First, we measured the loss of righting reflex (LRR) as a behavioral outcome, given the reported deficit induced by our model CHIMERA and its relevance to TBI serving as a predictor for symptom development and severity in TBI. Our results revealed an increase in LRR in the rmTBI groups (injury effect, ($F_{1, 51} = 15.07$, $p = 0.0003$), with the duration aligning with mild effect scale (LRR <15 min) (Fig. 2A). Importantly, aged mice demonstrated a more severe phenotype compared to their younger counterparts (age effect, ($F_{1, 51} = 19.50$, $p < 0.0001$). Group-specific LRR observations were not influenced by body weight (injury effect, ($F_{1, 51} = 0.067$, $p = 0.796$). (Fig. 2B). In functional images, we applied graph theory matrices to assess overall network integrity: network strength (indicating global connectivity, Fig. 2C), characteristic path length (information travel distance, Fig. 2D), global efficiency (overall communication, Fig. 2E) and small-world index (SWI; balancing local and global connectivity, Fig. 2F). In general, major global differences were not detected except for a significant decrease in SWI induced by aging (Y-Sh vs. A-Sh, $p < 0.0001$), indicating reduced global communication between various brain regions. However, injuries induced an opposing effect on SWI in different age groups (Interaction effect, ($F_{57, 518} = 1.746$, $p = 0.001$). A decreased in SWI indicate more segregation into specialized regions, where nodes form tight clusters while

maintaining short paths between distant nodes. rmTBI induced this effect in young mice (Y-Sh vs Y-TBI, $p < 0.0001$), while shifting towards more global integration in aged-injured animals (A-Sh vs A-TBI, $p < 0.001$).

3.2. Functional connectivity changes at local regions affected by age and treatment

We then inspected how 148 regions of interest (ROI, nodes) distributed throughout the brain were functionally connected or restructured by age or after injury. We found that 79 out of the 148 regions were altered by age (young vs. aged), injury (sham vs. rmTBI), or the interaction between these factors (Fig. 3; effect size for each ROI is provided in Supplemental Figure S1). Color-coded regions represent areas showing a statistically significant value ($p < 0.05$). Main effects by each ROI are included in Fig. 3A; listing those regions with at least 2 significant changes and substantial effect among the metrics. The most prominent changes were observed in eigenvector centrality, a metric that characterizes how age and rmTBI impact the number of connections and their influence on neighboring regions and community hubs in specific areas of the brain. Age emerged as the primary influencing factor on eigenvector centrality in 64 % of regions (Fig. 3B). Injuries exerted greater effects on areas critical for sensory integration and pain such as the entorhinal cortex and agranular insula (posterior and ventral areas). The total number of affected regions in left and right hemispheres was counted to detect any asymmetric measures (Fig. 3C). Interestingly, while fewer regions were affected in the left hemisphere, it's noteworthy that this side exhibited more pronounced connectivity changes when considering all metrics within these regions. Following TBI, interhemisphere functional connectivity of resting networks can be affected (Rigon et al., 2016). Thus, these lateralization differences might lead to inter-hemispheric disconnection. While betweenness centrality changes were equal, indicating disrupted communication nodes in both hemispheres, significant eigenvector centrality changes in the left hemisphere highlight an impact on key nodes. These changes can be attributed to individual variability and injury response, given the consistent impact location in our rmTBI model. We were unable to reliably assess sex differences; however, preliminary comparisons in Supplemental Figure S2 suggested distinct ROIs affected by these metrics, revealing a more significant impact of rmTBI and age factors on males. These findings emphasize the broad interplay of age, injury, and brain connectivity, providing a deeper understanding of numerous brain connections affected by TBIs.

3.3. Age, brain network reorganization, and injury effects

To further investigate these effects, we performed multiple comparisons test to pinpoint specific distinctions in brain regions among the groups (Fig. 4A). This analysis revealed that the injuries primarily increased eigenvector centrality and node strength in motor cortices in young mice (Fig. 4B). Conversely, in aged mice, injuries resulted in decline in both the number (degree) and strength of local connections within the brain. This suggests a diminished capacity for local interactions and communications. Additionally, these injuries affected the connections' influence on neighboring areas, potentially disrupting the overall network dynamics and communication between different regions of the brain of aged mice. In young mice, the only region that exhibited a reduction in node strength, node degree, and eigenvector centrality was the posterior agranular insula. In aged mice, the ventral segment of insula showed a decrease in the same measurements (l_vains, node strength, $p =$

0.0007; l_vains, eigenvector centrality, $p = 0.021$ Fig. 4C). Minor differences between young and aged sham (Y-Sh vs A-Sh) were detected where aging heightened activity in auditory (r_audv, betweenness, $p = 0.014$; r_audd, eigenvector centrality, 0.033), hippocampal (node strength in CA3 area, $p = 0.042$), while reducing number of connections in striatal areas (r_vms2, node degree, $p = 0.035$). In the hippocampal region (dentate gyrus), aged-injured mice revealed increased influence (r_hpc2, $p = 0.033$; r_hpc3, $p = 0.043$) and region strength (r_hpc3, $p = 0.034$) of functional connections relative to young-rmTBI mice. These observations confirm that the effect of repetitive brain injuries on brain connectivity varies significantly with age.

Mean connectivity broadly defines the degree of interconnections between these regions of interest within the brain network, whereas eigenvector centrality describes the quality and influence of these connections (Fig. 5A). Overall, global mean connectivity and eigenvector centrality revealed age-related differences, where aged mice exhibit denser connectivity in the caudal area while effects in young mice were concentrated in frontal regions. Higher edge densities signify a greater degree of connectivity. Two regions may have the same number of connections (nodes 1 and 2 in Fig. 5B); however, these regions can significantly differ in terms of information flow and influence within the network, as measured by eigenvector centrality. To gain further insight, we assessed eigenvector centrality by grouping ROIs into four subdivisions: hippocampal formation (HPC), thalamus, striatum, and isocortex (Fig. 5C). Quantitative analysis reveals a stark contrast in network reconfiguration between young and aged mice following injury (Fig. 5D–G). Specifically, the most influential regions concentrated in the isocortex and striatum for young mice and in the hippocampal and thalamic area for aged mice, respectively. These findings raise questions about the efficiency of information flow between the frontal cortex and thalamic regions, prompting us to investigate whether microstructural damage in brain tissue may be the contributing factor.

3.4. Age-related disruptions in white matter integrity

The impact of age and injury on diffusion of water molecules, as an indicator of white matter organization, was examined in 36 regions using DTI (Fig. 6A; effect size for each ROI is provided in Supplemental Figure S3). By measuring fractional anisotropy (FA), we inspected diffusion through white matter tracts in a single direction (FA =1, highly organized) or in all directions (FA = 0, tissue damage). Radial and axial diffusivity are sensitive to axonal disruption detecting the flow perpendicular (RD) or parallel (AD) to fiber tracts. Major age-dependent disruptions in diffusion manifested in the corticospinal tract, hippocampal commissure, anterior cingulate, and optic tract. Surprisingly, mean diffusivity (MD), which displays the overall diffusion of water in these regions, was affected uniquely by age (Fig. 6B). NODDI provided better insight into the density and orientation of axons in intracellular organization (axons and neurites; OD), intracellular fluid (volume occupied by neurites; ICVF) and extracellular (surrounding of neurites; ISOVF) compartments. As in DTI results, age remained as the determinant factor on the neurite density (Fig. 6B).

In control animals, the anterior cingulate, agranular insula, and retrosplenial areas showed a notable decrease in MD and RD due to aging (Fig. 7A). Conversely, the entorhinal cortex,

anterior cingulate, and optic tract were the areas affected in young mice. In line with previous studies, the optic tract was the top affected region showing changes in young and aged animals (Fig. 7A) (Sakthivel et al., 2023; Winklewski et al., 2018). Further analysis indicated that aging represents a general increase in fractional anisotropy (FA) and decreased RD when comparing young to aged animals. Independent of injuries, aged animals showed an inverse correlation between FA and RD in secondary motor area, corticospinal tract, and hippocampal commissure (Fig. 7B–D). This inverse relationship signifies a noticeable alteration in white matter integrity, distinguishing it from the young group. Interestingly, the interplay between age and injury had a discernible impact on diffusivity in the retrosplenial cortex, a region crucial for diverse processing within the limbic system (Fig. 7E–F). Overall, the observed FA/RD relationship is a well-supported indicator of demyelination and axonal damage (Winklewski et al., 2018). Consequently, we conducted additional assessments to explore inflammation as a potential mechanism driving axonal damage.

3.5. Neuroinflammation correlates with higher dispersion in the optic tract

Inflammation is a prevailing pathological response found in aged or injured brains (Sakthivel et al., 2023; Mouzon et al., 2018; Button et al., 2021). Injury increased levels of Iba-1 ($p = 0.0009$) and GFAP ($p = 0.0005$) inflammatory markers in the optic tract of aged animals (Fig. 8A–D). The upregulation of these markers in the optic tract suggests a concerted effort of the immune system to respond to injury-induced stress, implying potential implications for the integrity and function of this neural pathway. For instance, neuroinflammation and neurodegeneration in the optic tract can coincide with damage in other areas like in thalamic nuclei affecting this pathway communication (Evanson et al., 2018).

4. Discussion

In this study, we investigated alterations in functional connectivity and white matter integrity resulting from rmTBI and aging. We established that major differences in these conditions were not global (Fig. 2); instead, a more granular evaluation of networks is necessary to define these changes, which in turn underlie the effects of age and head injury on brain health. We established that SWI is reduced by injury (in young animals) and age, disrupting the balance between local clustering and global integration, thereby affecting communication across the entire network. Our observations align with findings in healthy individuals, where global efficiency remains unchanged while changes are detected at local level by decreasing regions efficiency with aging (Song et al., 2014). In the context of mild TBI, it is essential to emphasize that symptoms and visible signs of injuries can manifest days after the event. These effects could intensify and persist for months (Kim et al., 2022; Bachstetter et al., 2020). Undetectable global changes, as revealed in this study, may contribute to why conventional clinical interventions often overlook and fail to accurately diagnose brain damage resulting from concussions or repetitive subconcussive hits, within the first days post-injury. Our findings corroborate in more granular detail that repetitive head injuries alter numerous brain regions leading to reorganization of the entire brain network (Sakthivel et al., 2023). More importantly, our results show that brain network restructuring occurs differently between young and aged mice. For instance, young animals primarily exhibited alterations in frontal-motor areas, whereas aged mice showed changes

in the agranular insula. A study in healthy young and aged individuals indicated that while global connectivity remains unchanged, the intermodular connections differ by age groups (Song et al., 2014). This local hub reorganization positively correlates with early symptoms of cognitive impairments following mTBI (Li et al., 2022). Highlighting contrasting areas affected by rmTBI may predict rmTBI-associated manifestations in behavior and cognition.

The observation of age-related changes in the functioning of the insula is important, given its role in integrating sensory, emotional, cardiovascular and motor functions (Menon and Uddin, 2010). The insula is strongly interconnected with the well-established default mode network, often referred to as a “resting state network” (Menon and Uddin, 2010; Centanni et al., 2021). Furthermore, aging is linked with declined default-mode network, reduced motor performance, and weakened frontal cortex connections, which are all associated with insular cortex function (Nyberg et al., 2010; Menon and Uddin, 2010; Grady et al., 2016; Jockwitz and Caspers, 2021). Furthermore, abnormally reduced connections within the anterior cingulate cortex are anticipated with aging. Similar reductions along with decreased segregation and local efficiency are also observed in healthy individuals without injury (Song et al., 2014; Varangis et al., 2019). Additional studies support that aging reduces default-mode network connectivity, motor performance, and frontal cortex connections (Nyberg et al., 2010; Grady et al., 2016; Jockwitz and Caspers, 2021).

It is plausible that the age-related variations we observed in this study are linked to reduced motor plasticity and tissue atrophy in the older cohort, consistent with the effects of aging (Mouzon et al., 2018; Liu et al., 2013; Ghasemian-Shirvan et al., 2020). Also, age-related changes in the anterior cingulate cortex impact connectivity between these crucial brain network hubs. Young animals exhibited higher FA and lower RD in ventral anterior cingulate cortex, which is related to improved organization and connectivity in white matter tracts. These changes were absent in aged mice. Two potential explanations are that 1) young animals have a higher degree of plasticity to compensate lost connections following injury and 2) age limits plasticity in the anterior cingulate cortex or motor cortex. Hence, the predominant rmTBI-effects observed in white matter integrity were found in young mice, possibly attributable to pre-existing damage in aged brains. Interestingly, the interplay between aging and injury, rather than each factor individually, significantly influenced tissue diffusion in key limbic regions - the amygdala (BLA), hippocampus (CA area), and posterior insula (Fig. 7A). These regions play pivotal roles in emotional responses, spatial learning, declarative memory formation, and sensory integration (encompassing awareness of both internal and external bodily states). Our results affirm that the concurrent influence of age and injury leads to more profound damage in emotional and cognitive processes.

Observations suggest the involvement of thalamic nuclei in conveying age-related connectivity differences. In young mice, the motor cortex and neighboring frontal regions showed increased reorganization. Conversely, aged animals exhibited higher integration (eigenvector centrality) in the thalamic area. Intriguingly, the insular cortex, whose centrality was reduced after rmTBI in aged mice, also shares bidirectional connections with both motor and thalamic areas (Gehrlach et al., 2020). The motor cortex and thalamus are not only functionally connected through lifespan, but also play pivotal roles in learning and decision-making (Inagaki et al., 2022; Wolff et al., 2022). Thalamic hyperconnectivity

correlates with chronic symptoms in mTBI patients, suggesting that early changes in thalamic nuclei may increase vulnerability to injury (Woodrow et al., 2023). Even without injury, aging impacts the thalamus in healthy subjects by reducing its volume as well as reducing projections to frontal areas, seen during resting or cognitive tasks (Nyberg et al., 2010; Hughes et al., 2012). Consequently, disruption in thalamic-cortical communication can be the underline root for the dissociation in centrality observed in this study.

Other cellular and molecular processes may be implicated in brain connectivity outcomes. For instance, neuroinflammation, oxidative stress, and neuronal loss are common effects related to aging (Button et al., 2021). All these processes are more pronounced in aged brains making them susceptible to damage, dissociation connections, and affecting the capacity to recovery (Sandhir et al., 2008; Anderson et al., 2009). Particularly, inflammation in the optic tract likely affects the visual and sensory input integration. This is noteworthy because reduced visual acuity, altered visual processing, and other eye conditions are more prevalent in elderly individuals. Also, higher inflammation in the optic tract might underlie visual impairment after injury and other symptoms like insomnia, attention deficits, and memory problems. Enhanced connectivity in this area could serve as a compensatory response to inflammation or a temporary adjustment during the initial days after injury. This could explain the mild symptoms in vision during early days as the brain adjusts.

Our study details how rmTBI affects brain network restructuring differently between young and aged mice, supporting the need of age-specific interventions and recovery strategies. We use CHIMERA model which replicates various aspects of human TBI and can be combined with imaging tools to provide value in both preclinical and clinical settings. Unlike other TBI models, CHIMERA reproduces rotational forces seen in human TBI, a major cause of diffuse axonal injury (McNamara et al., 2020). Other phenotypes are shared with TBI models such as the closed-head weight-drop, controlled cortical impact, and CHIMERA. For instance, young mice subjected to the closed-head weight-drop model exhibit diffuse axonal injury, neuroinflammation, and disrupted network connectivity (Meningher et al., 2020). The controlled cortical impact model results in severe neurodegeneration and cognitive deficits (Xu et al., 2021). The CHIMERA model induces neuroinflammation, cognitive deficits, axonal damage, and neurodegeneration markers like tau protein (Sakthivel et al., 2023; Cheng et al., 2019; Chen et al., 2017). These comparisons highlight the multifaceted nature of mTBI and emphasize the need for tailored therapeutic approaches based on specific injury mechanisms and age-related vulnerabilities. The symptoms and pathologies observed align with clinical TBI cases, aiding in a better understanding of the consequences of brain damage with respect to age and timing of diagnosis.

4.1. Future studies and limitations

Whether the centrality observed in the thalamus of aged mice results from damaged connections remain uncertain. Ongoing studies to investigate whether centrality represents a compensatory mechanism or delayed communication between thalamic-frontal connections are underway. Further insights can be gained by assessing different thalamic and main connecting tracts, like corpus callosum, to pinpoint specific regions responsible for the dissociation between frontal and thalamic connectivity. Notably, there has been a greater

number of longitudinal studies conducted in young rodents compared to aged mice. The present study is one of limited investigations assessing changes at 22 months of age. This presents challenges in predicting and comparing long-term effects in this age group. Also, the onset of strain-related diseases occurring beyond this time point can be misleading of the true impact of injury. Discussions regarding the lasting effects by rmTBI have been postulated in recent years. This is because others using closed-head injuries detect recovery after a month following the injury event (Yang et al., 2015; Yang et al., 2021). However, here we use the surgery-free CHIMERA model which produces lasting effects in tissue pathology, imaging, neurophysiology, and behavior (McNamara et al., 2020; Cheng et al., 2019; Chen et al., 2017). Moreover, we intended to explore sex differences, but exclusion of images with motion artifacts in some groups impacted the sample size, hindering statistical power for assessing this factor. The contribution of sex in our findings is interesting for further exploration because deficits in the thalamus and motor cortex are known to be impacted by sex and age. Particularly, adolescent males are susceptible to these factors following rmTBI, showing deficits in motor function linked to reduced microglia density in these areas (Eyolfson et al., 2020). Lastly, to enhance the translational value of our findings, it would be advantageous to link them with other brain and blood markers.

5. Conclusion

In summary, our study reveals age-specific changes in brain connectivity and white matter properties following multiple mild traumatic brain injuries. Using a multi-modal approach, we identify reduced communication efficiency and contrasting effects on the small-world index, influencing network segregation with age. These discoveries shed light on the intricate interactions between age, injuries, and brain connectivity, offering implications for understanding the solid effects of rmTBIs in the context of aging and the potential early pathological features that may develop to neurodegeneration and contribute to impairment of brain functions.

Transparency, rigor, and reproducibility

For imaging studies, the total sample size was 32 consisting of Young-Sham ($n = 8$), Young-rmTBI ($n = 10$), Aged-Sham ($n = 6$), and Aged-rmTBI ($n = 8$). For IHC experiment in aged mice, the total sample size was 19 (Sham, $n = 10$; rmTBI, $n = 9$). Animals were randomly assigned to experimental groups, and the injury procedures and imaging processing were designed and conducted with blinding. Information about the animals' group assignments was not revealed until the statistical analyses were conducted. Data were submitted in a BioRxiv preprint.

Supplementary Material

Refer to Web version on PubMed Central for supplementary material.

Acknowledgements

We thank David R. Borchelt and Susan Fromholt for their invaluable contribution in supplying the aged animals, crucial for the successful completion of this study. The main funding for this project was provided by NIH/NIA grant 1 R01 AG074584–01 and partial support from the NIH grant S10 RR025671 for MRI/S instrumentation.

We extend our gratitude to the Alzheimer's Association for the 2019-AARFD-644407 fellowship grant, awarded to Marangelie Criado-Marrero, which greatly supported her training and the research findings detailed in this publication. A portion of the experiments were conducted at the McKnight Brain Institute, within the Advanced Magnetic Resonance Imaging and Spectroscopy (AMRIS) Facility at the National High Magnetic Field Laboratory. This facility was made possible through additional support from the National Science Foundation Cooperative Agreement DMR-1644779 and the State of Florida.

Data availability

Data will be made available on request.

References

Abisambra JF, Scheff S, 2014. Brain injury in the context of tauopathies. J. Alzheimers Dis 40, 495–518. 10.3233/JAD-131019. [PubMed: 24496078]

Anderson J, Sandhir R, Hamilton ES, Berman NE, 2009. Impaired expression of neuroprotective molecules in the HIF-1alpha pathway following traumatic brain injury in aged mice. J. Neurotrauma 26, 1557–1566. 10.1089/neu.2008.0765. [PubMed: 19203226]

Bachstetter AD, et al. , 2020. The effects of mild closed head injuries on tauopathy and cognitive deficits in rodents: primary results in wild type and rTg4510 mice, and a systematic review. Exp. Neurol 326, 113180 10.1016/j.expneurol.2020.113180. [PubMed: 31930992]

Berman R, et al. , 2023. Loss of consciousness and righting reflex following traumatic brain injury: predictors of post-injury symptom development (A Narrative Review). Brain Sci 13. 10.3390/brainsci13050750.

Button EB, et al. , 2021. Development of a novel, sensitive translational immunoassay to detect plasma glial fibrillary acidic protein (GFAP) after murine traumatic brain injury. Alzheimers Res. Ther 13, 58. 10.1186/s13195-021-00793-9. [PubMed: 33678186]

Centanni SW, Janes AC, Haggerty DL, Atwood B, Hopf FW, 2021. Better living through understanding the insula: why subregions can make all the difference. Neuropharmacology 198, 108765. 10.1016/j.neuropharm.2021.108765. [PubMed: 34461066]

Centers for Disease Control and Prevention, http://wonder.cdc.gov/ (2023).

Chen H, Desai A, Kim HY, 2017. Repetitive closed-head impact model of engineered rotational acceleration induces long-term cognitive impairments with persistent astrogliosis and microgliosis in mice. J. Neurotrauma 34, 2291–2302. 10.1089/neu.2016.4870. [PubMed: 28288551]

Cheng WH, et al. , 2019. CHIMERA repetitive mild traumatic brain injury induces chronic behavioural and neuropathological phenotypes in wild-type and APP/PS1 mice. Alzheimers Res. Ther 11, 6. 10.1186/s13195-018-0461-0. [PubMed: 30636629]

Coelho A, et al. , 2021. Signatures of white-matter microstructure degradation during aging and its association with cognitive status. Sci. Rep 11, 4517. 10.1038/s41598-021-83983-7. [PubMed: 33633204]

Colon-Perez LM, et al. , 2019. Neurite orientation dispersion and density imaging reveals white matter and hippocampal microstructure changes produced by Interleukin-6 in the TgCRND8 mouse model of amyloidosis. Neuroimage 202, 116138. 10.1016/j.neuroimage.2019.116138. [PubMed: 31472250]

Cox RW, 1996. AFNI: software for analysis and visualization of functional magnetic resonance neuroimages. Comput. Biomed. Res 29, 162–173. 10.1006/cbmr.1996.0014. [PubMed: 8812068]

Daducci A, et al. , 2015. Accelerated microstructure imaging via convex optimization (AMICO) from diffusion MRI data. Neuroimage 105, 32–44. 10.1016/j.neuroimage.2014.10.026. [PubMed: 25462697]

D'Souza MM, et al. , 2020. Alterations of connectivity patterns in functional brain networks in patients with mild traumatic brain injury: a longitudinal resting-state functional magnetic resonance imaging study. Neuroradiol. J 33, 186–197. 10.1177/1971400920901706. [PubMed: 31992126]

Evanson NK, Guilhaume-Correa F, Herman JP, Goodman MD, 2018. Optic tract injury after closed head traumatic brain injury in mice: a model of indirect traumatic optic neuropathy. PLoS ONE 13, e0197346. 10.1371/journal.pone.0197346. [PubMed: 29746557]

Eyolfson E, et al. , 2020. Repetitive mild traumatic brain injuries in mice during adolescence cause sexually dimorphic behavioral deficits and neuroinflammatory dynamics. J. Neurotrauma 37, 2718–2732. 10.1089/neu.2020.7195. [PubMed: 32772786]

Gardner RC, Dams-O'Connor K, Morrissey MR, Manley GT, 2018. Geriatric traumatic brain injury: epidemiology, outcomes, knowledge gaps, and future directions. J. Neurotrauma 35, 889–906. 10.1089/neu.2017.5371. [PubMed: 29212411]

Garza N, Toussi A, Wilson M, Shahlaie K, Martin R, 2020. The increasing age of TBI patients at a single level 1 trauma center and the discordance between GCS and CT Rotterdam scores in the elderly. Front. Neurol 11, 112. 10.3389/fneur.2020.00112. [PubMed: 32153493]

Gehrlach DA, et al. , 2020. A whole-brain connectivity map of mouse insular cortex. Elife 9. 10.7554/eLife.55585.

Ghasemian-Shirvan E, et al. , 2020. Age-related differences of motor cortex plasticity in adults: a transcranial direct current stimulation study. Brain Stimul 13, 1588–1599. 10.1016/j.brs.2020.09.004. [PubMed: 32949779]

Grady C, Sarraf S, Saverino C, Campbell K, 2016. Age differences in the functional interactions among the default, frontoparietal control, and dorsal attention networks. Neurobiol. Aging 41, 159–172. 10.1016/j.neurobiolaging.2016.02.020. [PubMed: 27103529]

Guan B, Anderson DB, Chen L, Feng S, Zhou H, 2023. Global, regional and national burden of traumatic brain injury and spinal cord injury, 1990–2019: a systematic analysis for the Global Burden of Disease Study 2019. BMJ Open 13, e075049. 10.1136/bmjopen-2023-075049.

Gugger JJ, et al. , 2023. Structural brain network deviations predict recovery after traumatic brain injury. Neuroimage Clin 38, 103392 10.1016/j.nicl.2023.103392. [PubMed: 37018913]

Hou Y, et al. , 2019. Ageing as a risk factor for neurodegenerative disease. Nat. Rev. Neurol 15, 565–581. 10.1038/s41582-019-0244-7. [PubMed: 31501588]

Hughes EJ, et al. , 2012. Regional changes in thalamic shape and volume with increasing age. Neuroimage 63, 1134–1142. 10.1016/j.neuroimage.2012.07.043. [PubMed: 22846656]

Inagaki HK, et al. , 2022. A midbrain-thalamus-cortex circuit reorganizes cortical dynamics to initiate movement. Cell 185, 1065–1081. 10.1016/j.cell.2022.02.006 e1023. [PubMed: 35245431]

Jockwitz C, Caspers S, 2021. Resting-state networks in the course of aging-differential insights from studies across the lifespan vs. amongst the old. Pflugers. Arch 473, 793–803. 10.1007/s00424-021-02520-7. [PubMed: 33576851]

Khong E, Odenwald N, Hashim E, Cusimano MD, 2016. Diffusion tensor imaging findings in post-concussion syndrome patients after mild traumatic brain injury: a systematic review. Front. Neurol 7, 156. 10.3389/fneur.2016.00156. [PubMed: 27698651]

Kim E, et al. , 2022. An exploratory study on functional connectivity after mild traumatic brain injury: preserved global but altered local organization. Brain Behav 12, e2735. 10.1002/brb3.2735. [PubMed: 35993893]

Li F, et al. , 2022. Rich-club reorganization of functional brain networks in acute mild traumatic brain injury with cognitive impairment. Quant. ImAging Med. Surg 12, 3932–3946. 10.21037/qims-21-915. [PubMed: 35782237]

Liu Y, Cao C, Yan JH, 2013. Functional aging impairs the role of feedback in motor learning. Geriatr. Gerontol. Int 13, 849–859. 10.1111/ggi.12013. [PubMed: 23551381]

Livingston DH, et al. , 2005. Recovery at one year following isolated traumatic brain injury: a Western Trauma Association prospective multicenter trial. J. Trauma 59, 1298–1304. 10.1097/01.ta.0000196002.03681.18 discussion 1304. [PubMed: 16394900]

Luo L, et al. , 2023. Depressive symptoms following traumatic brain injury are associated with resting-state functional connectivity. Psychol. Med 53, 2698–2705. 10.1017/S0033291721004724. [PubMed: 37310305]

McNamara EH, Grillakis AA, Tucker LB, McCabe JT, 2020. The closed-head impact model of engineered rotational acceleration (CHIMERA) as an application for traumatic brain injury pre-clinical research: a status report. Exp. Neurol 333, 113409 10.1016/j.expneurol.2020.113409. [PubMed: 32692987]

Meningher I, Bernstein-Eliav M, Rubovitch V, Pick CG, Tavor I, 2020. Alterations in network connectivity after traumatic brain injury in mice. J. Neurotrauma 37, 2169–2179. 10.1089/neu.2020.7063. [PubMed: 32434427]

Menon V, Uddin LQ, 2010. Saliency, switching, attention and control: a network model of insula function. Brain Struct. Funct 214, 655–667. 10.1007/s00429-010-0262-0. [PubMed: 20512370]

Mohamed AZ, Cumming P, Nasrallah FA, Department of Defense Alzheimer's Disease Neuroimaging Initiative, 2021. White matter alterations are associated with cognitive dysfunction decades after moderate-to-severe traumatic brain injury and/or posttraumatic stress disorder. Biol. Psychiatry Cogn. Neurosci. NeuroimAging 6, 1100–1109. 10.1016/j.bpsc.2021.04.014. [PubMed: 33957321]

Moreira da Silva N, Cowie CJA, Blamire AM, Forsyth R, Taylor PN, 2020. Investigating brain network changes and their association with cognitive recovery after traumatic brain injury: a longitudinal analysis. Front. Neurol 11, 369. 10.3389/fneur.2020.00369. [PubMed: 32581989]

Mouzon BC, et al. , 2018. Lifelong behavioral and neuropathological consequences of repetitive mild traumatic brain injury. Ann. Clin. Transl. Neurol 5, 64–80. 10.1002/acn3.510. [PubMed: 29376093]

Namjoshi DR, et al. , 2014. Merging pathology with biomechanics using CHIMERA (Closed-Head Impact Model of Engineered Rotational Acceleration): a novel, surgery-free model of traumatic brain injury. Mol. Neurodegener 9, 55. 10.1186/1750-1326-9-55. [PubMed: 25443413]

Namjoshi DR, et al. , 2017. Defining the biomechanical and biological threshold of murine mild traumatic brain injury using CHIMERA (Closed Head Impact Model of Engineered Rotational Acceleration). Exp. Neurol 292, 80–91. 10.1016/j.expneurol.2017.03.003. [PubMed: 28274861]

Nyberg L, et al. , 2010. Longitudinal evidence for diminished frontal cortex function in aging. Proc. Natl. Acad. Sci. U.S.A 107, 22682–22686. 10.1073/pnas.1012651108. [PubMed: 21156826]

Onyszchuk G, He YY, Berman NE, Brooks WM, 2008. Detrimental effects of aging on outcome from traumatic brain injury: a behavioral, magnetic resonance imaging, and histological study in mice. J. Neurotrauma 25, 153–171. 10.1089/neu.2007.0430. [PubMed: 18260798]

Palacios EM, et al. , 2017. Resting-state functional connectivity alterations associated with six-month outcomes in mild traumatic brain injury. J. Neurotrauma 34, 1546–1557. 10.1089/neu.2016.4752. [PubMed: 28085565]

Pavlov V, et al. , 2019. Mild traumatic brain injury in the United States: demographics, brain imaging procedures, health-care utilization and costs. Brain Inj 33, 1151–1157. 10.1080/02699052.2019.1629022. [PubMed: 31241427]

Pompilus M, Colon-Perez LM, Grudny MM, Febo M, 2020. Contextual experience modifies functional connectome indices of topological strength and efficiency. Sci. Rep 10, 19843. 10.1038/s41598-020-76935-0. [PubMed: 33199790]

Powell JM, Ferraro JV, Dikmen SS, Temkin NR, Bell KR, 2008. Accuracy of mild traumatic brain injury diagnosis. Arch. Phys. Med. Rehabil 89, 1550–1555. 10.1016/j.apmr.2007.12.035. [PubMed: 18597735]

Rigon A, Duff MC, McAuley E, Kramer AF, Voss MW, 2016. Is traumatic brain injury associated with reduced inter-hemispheric functional connectivity? A study of large-scale resting state networks following traumatic brain injury. J. Neurotrauma 33, 977–989. 10.1089/neu.2014.3847. [PubMed: 25719433]

Sakthivel R, et al. , 2023. Fixed time-point analysis reveals repetitive mild traumatic brain injury effects on resting state functional magnetic resonance imaging connectivity and neuro-spatial protein profiles. J. Neurotrauma 40, 2037–2049. 10.1089/neu.2022.0464. [PubMed: 37051703]

Salottolo K, Levy AS, Slone DS, Mains CW, Bar-Or D, 2014. The effect of age on Glasgow Coma Scale score in patients with traumatic brain injury. JAMa Surg 149, 727–734. 10.1001/jamasurg.2014.13. [PubMed: 24899145]

Sandhir R, Onyszchuk G, Berman NE, 2008. Exacerbated glial response in the aged mouse hippocampus following controlled cortical impact injury. Exp. Neurol 213, 372–380. 10.1016/j.expneurol.2008.06.013. [PubMed: 18692046]

Smith SM, et al. , 2004. Advances in functional and structural MR image analysis and implementation as FSL. Neuroimage 23 Suppl 1, S208–S219. 10.1016/j.neuroimage.2004.07.051. [PubMed: 15501092]

Smolen P, Dash PK, Redell JB, 2023. Traumatic brain injury-associated epigenetic changes and the risk for neurodegenerative diseases. Front. Neurosci 17, 1259405 10.3389/fnins.2023.1259405. [PubMed: 37795186]

Song J, et al. , 2014. Age-related reorganizational changes in modularity and functional connectivity of human brain networks. Brain Connect 4, 662–676. 10.1089/brain.2014.0286. [PubMed: 25183440]

Timaru-Kast R, et al. , 2012. Influence of age on brain edema formation, secondary brain damage and inflammatory response after brain trauma in mice. PLoS ONE 7, e43829. 10.1371/journal.pone.0043829. [PubMed: 22952778]

Tournier JD, et al. , 2019. MRtrix3: a fast, flexible and open software framework for medical image processing and visualisation. Neuroimage 202, 116137. 10.1016/j.neuroimage.2019.116137. [PubMed: 31473352]

Varangis E, Habeck CG, Razlighi QR, Stern Y, 2019. The effect of aging on resting state connectivity of predefined networks in the brain. Front. Aging Neurosci 11, 234. 10.3389/fnagi.2019.00234. [PubMed: 31555124]

Wang Q, et al. , 2020. The allen mouse brain common coordinate framework: a 3D reference atlas. Cell 181, 936–953. 10.1016/j.cell.2020.04.007 e920. [PubMed: 32386544]

Winklewski PJ, et al. , 2018. Understanding the physiopathology behind axial and radial diffusivity changes-what do we know? Front. Neurol 9, 92. 10.3389/fneur.2018.00092. [PubMed: 29535676]

Wolff SBE, Ko R, Olveczky BP, 2022. Distinct roles for motor cortical and thalamic inputs to striatum during motor skill learning and execution. Sci. Adv 8, eabk0231. 10.1126/sciadv.abk0231. [PubMed: 35213216]

Woodrow RE, et al. , 2023. Acute thalamic connectivity precedes chronic post-concussive symptoms in mild traumatic brain injury. Brain 146, 3484–3499. 10.1093/brain/awad056. [PubMed: 36811945]

Xia M, Wang J, He Y, 2013. BrainNet Viewer: a network visualization tool for human brain connectomics. PLoS ONE 8, e68910. 10.1371/journal.pone.0068910. [PubMed: 23861951]

Xu X, et al. , 2021. Repetitive mild traumatic brain injury in mice triggers a slowly developing cascade of long-term and persistent behavioral deficits and pathological changes. Acta Neuropathol. Commun 9, 60. 10.1186/s40478-021-01161-2. [PubMed: 33823944]

Yang Z, et al. , 2015. Temporal MRI characterization, neurobiochemical and neurobehavioral changes in a mouse repetitive concussive head injury model. Sci. Rep 5, 11178. 10.1038/srep11178. [PubMed: 26058556]

Yang Z, et al. , 2021. Compensatory functional connectome changes in a rat model of traumatic brain injury. Brain Commun 3, fcab244. 10.1093/braincomms/fcab244. [PubMed: 34729482]

Yushkevich PA, et al. , 2006. User-guided 3D active contour segmentation of anatomical structures: significantly improved efficiency and reliability. Neuroimage 31, 1116–1128. 10.1016/j.neuroimage.2006.01.015. [PubMed: 16545965]

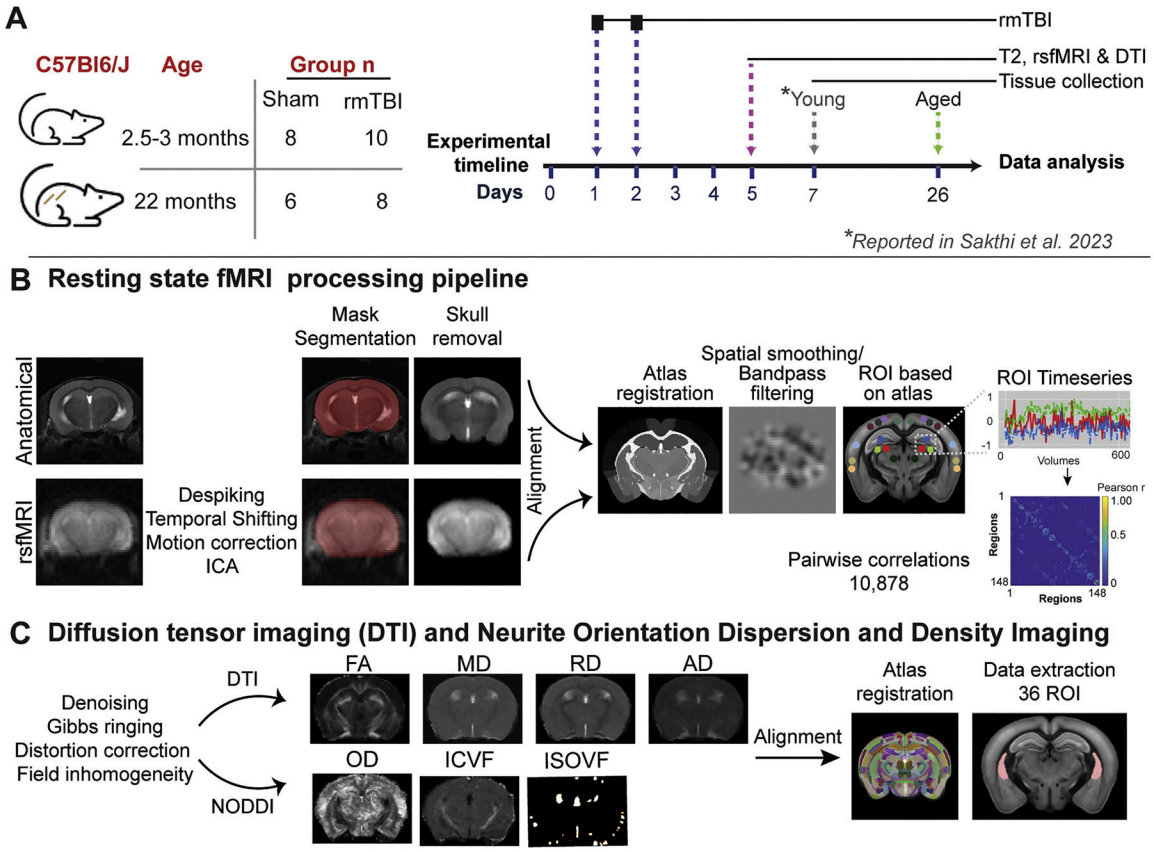

Fig. 1.

Experimental design and neuroimaging analysis. (A) Schematic representation showing the number of repetitive mild traumatic brain injuries (rmTBI), rsfMRI and tissue collection. (B) Resting state functional MRI processing pipeline. (C) Diffusion tensor imaging (DTI) and neurite orientation dispersion and density imaging (NODDI) workflow. ROI, region of interest; rsfMRI, resting-state functional magnetic resonance imaging; ICA, independent component analysis; FA, fractional anisotropy; MD, mean diffusivity; AD, axial diffusivity; RD, radial diffusivity; ISOVF, isotropic volume fraction; ICVF, intracellular volume fraction; OD, orientation dispersion index.

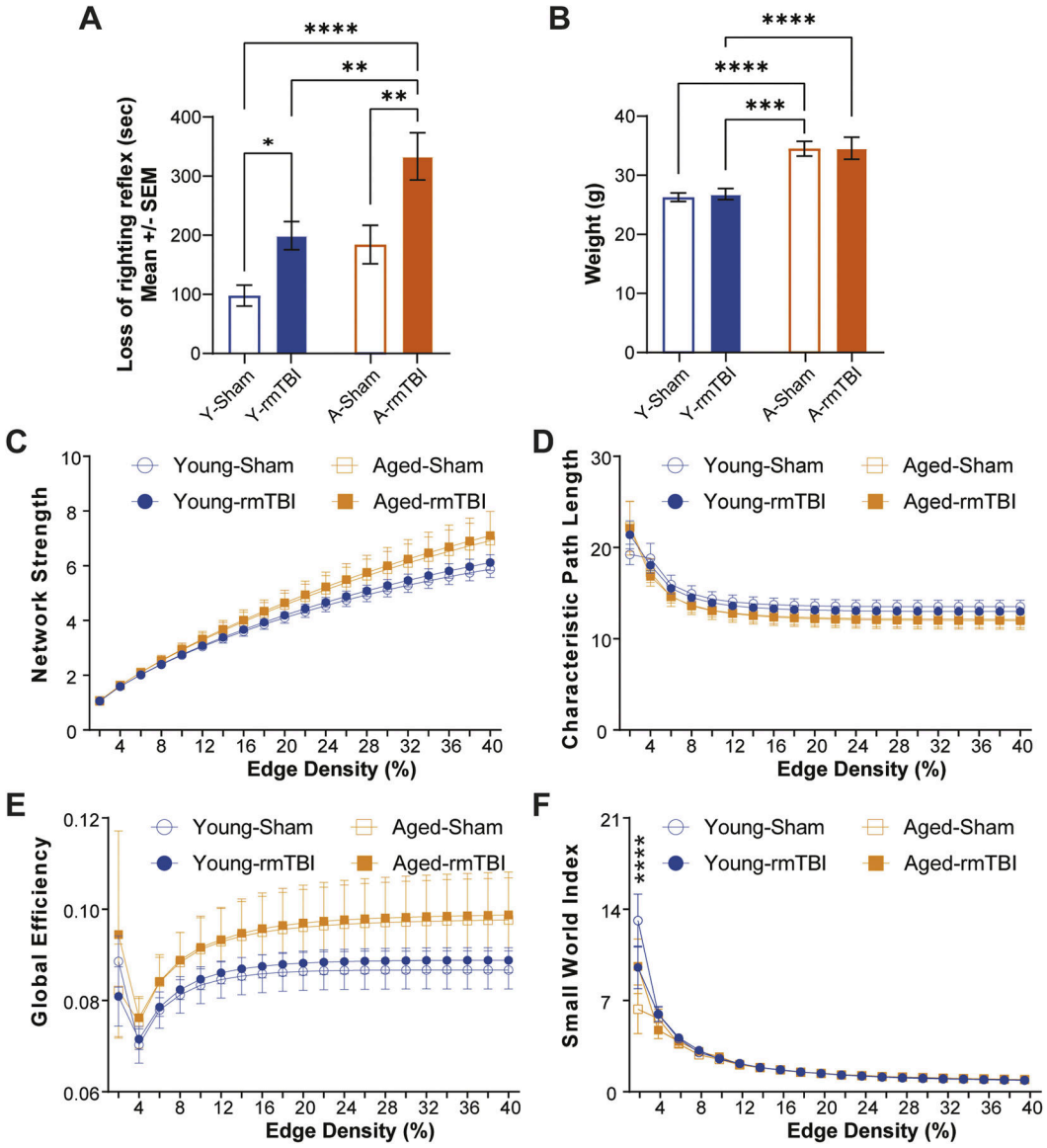

Fig. 2.

Global network changes in young and aged mice. TBI-related physiological symptoms were assessed immediately after injury. (A) In rmTBI groups, there was a higher loss of righting reflex (LRR), serving as a rodent analog to loss of consciousness in humans. Aged mice exhibited a more severe phenotype compared to young mice. (B) rmTBI-induced effects in LRR were independent of weight. Brain network was assessed by using (C) network strength (measures overall network connectivity), (D) characteristic path length (quantifies network communication efficiency), (E) global efficiency (assesses information transmission efficiency), and (F) small-world index (SWI, evaluates local and global information balance). Two-way ANOVA was conducted in LRR and weight measurements while repeated measures two-way ANOVA were used in network analyses examining a range from 2 to 40 edge density thresholds. Statistically significant difference is indicated as

*$p < 0.05$, **$p < 0.01$, ***$p < 0.001$, ****$p < 0.0001$. rmTBI, repetitive mild trauma brain injury; Y, young; A, Aged; *sec*, seconds; g, grams.

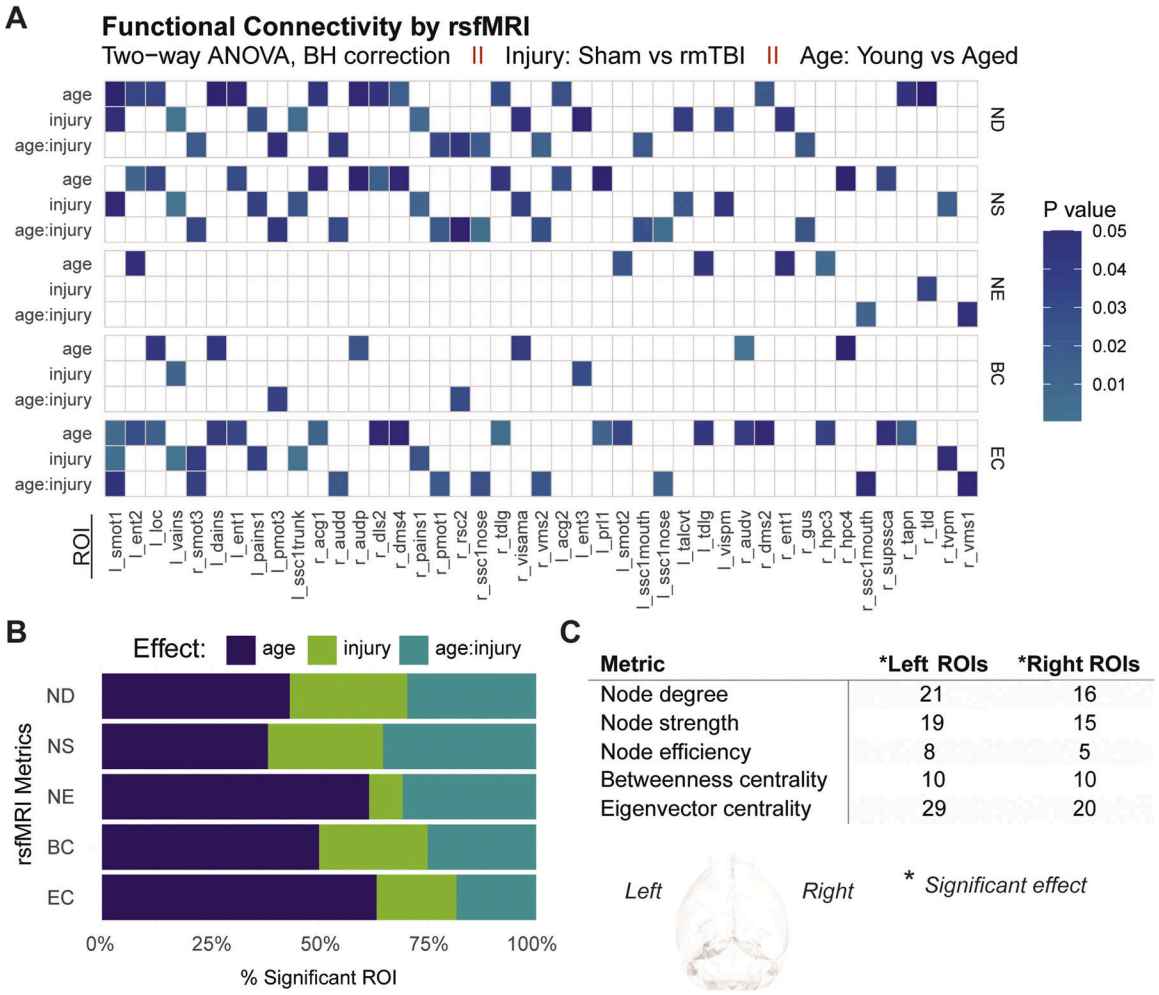

Metric	*Left ROIs	*Right ROIs
Node degree	21	16
Node strength	19	15
Node efficiency	8	5
Betweenness centrality	10	10
Eigenvector centrality	29	20

Fig. 3.

Age and treatment effects on rsfMRI metrics in brain. A threshold of 10 % edge density was applied for local analyses, which is within the most robust and least dense connections. (A) Main effects and interaction of age and injury (injury = sham vs rmTBI) on the following rsfMRI metrics: node degree (ND), node strength (NS), node efficiency (NE), betweenness centrality (BC), and eigenvector centrality (EC). Out of the 148 regions of interest evaluated, only those with 2 or more significant values are represented in the heatplot. Statistically significant ($p < 0.05$) effects for each region of interest (ROI) resulting from Type III two-way ANOVA with Benjamini false discovery rate (FDR-BH) correction are represented in color. White squares denote non-significant values. (B) Percentage of significant ROI affected by age, injury, interaction age and injury for each metric. (C) Significant main effects distribution in right and left-brain hemisphere. rsfMRI = resting-state functional magnetic resonance imaging. ROI names are detailed in Supplemental Table 1.

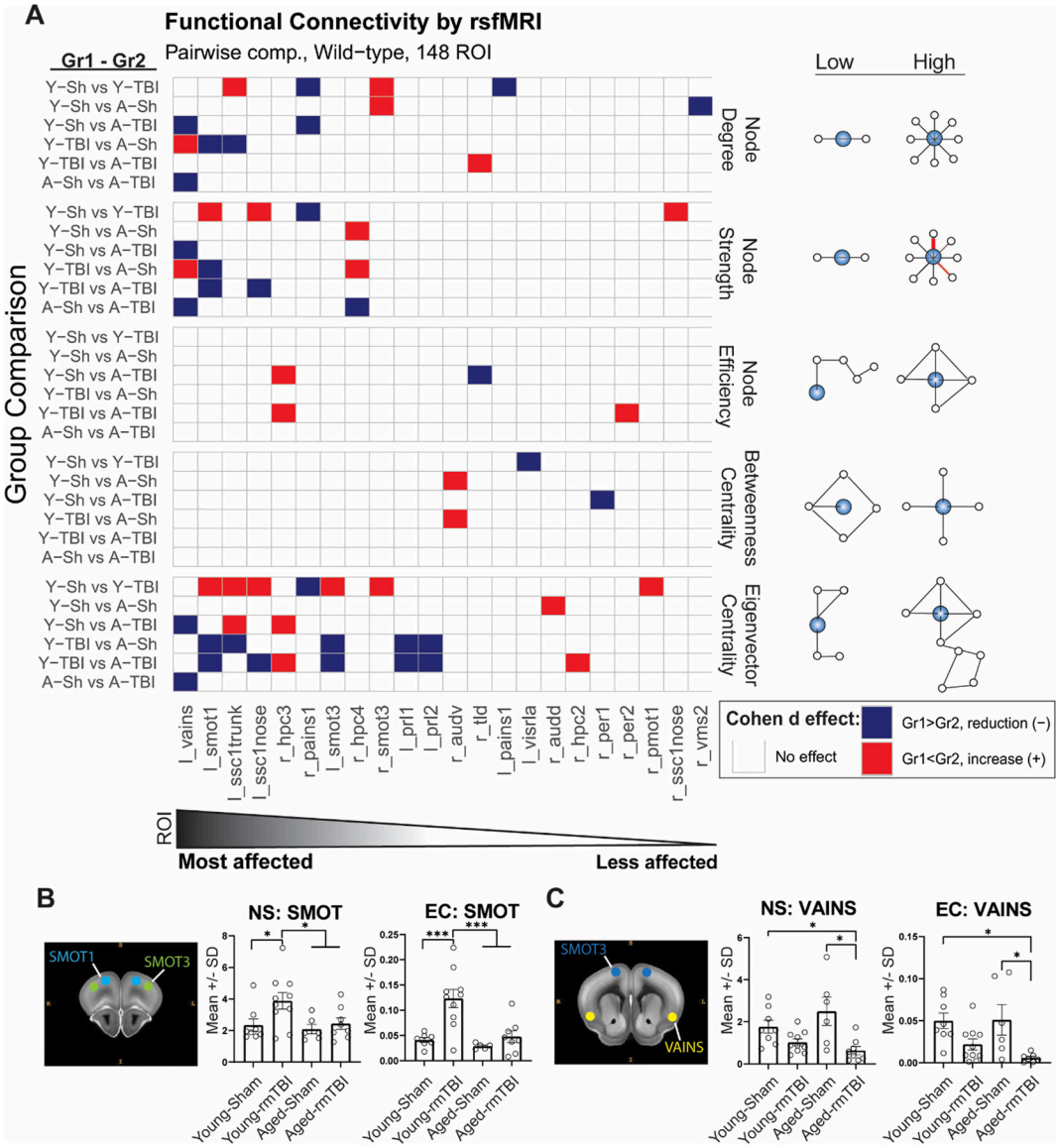

Fig. 4.

Multiple comparison and effect sizes on top affected brain regions in young and aged mice after rmTBI. (A) Multiple comparisons tests were conducted on the regions of interest (ROI) showing significant main effects in the two-way ANOVA. Adjusted *p*-values resulting from pairwise comparisons with Benjamini-Hochberg (FDR-BH) correction are color-coded in the heatplot. The magnitude and direction of the effect were determined by Cohen's d effect size. Red represents an effect size equal to or greater (red) or lower (blue) than +/−0.8 (large effect). ROIs are arranged from left to right based on the highest number of significant *p*-values across metrics. Diagrams on the right illustrate scores assigned to a region of interest (ROI, blue circle) based on its connectivity to other regions (white circles), ranging from low to high values. (B) In young mice, the secondary motor area (left smot1) exhibited the greatest impact by rmTBI, while (C) in the aged group, the ventral agranular insula (left vains) emerged as the most affected region. NS = node strength,

EC = eigenvector centrality. Bar graphs represent the mean with standard deviation (SD). Statistically significant *p*-values from two-way ANOVA are represented as follows: $*p < 0.05$, $***p < 0.001$. Gr1, group1 is first from left to right in panel; Young-Sham (Y-Sh), $n = 8$; Young-rmTBI (Y-TBI), $n = 10$; Aged-Sham (A-Sh), $n = 6$; Aged-rmTBI (A-TBI), $n = 8$.

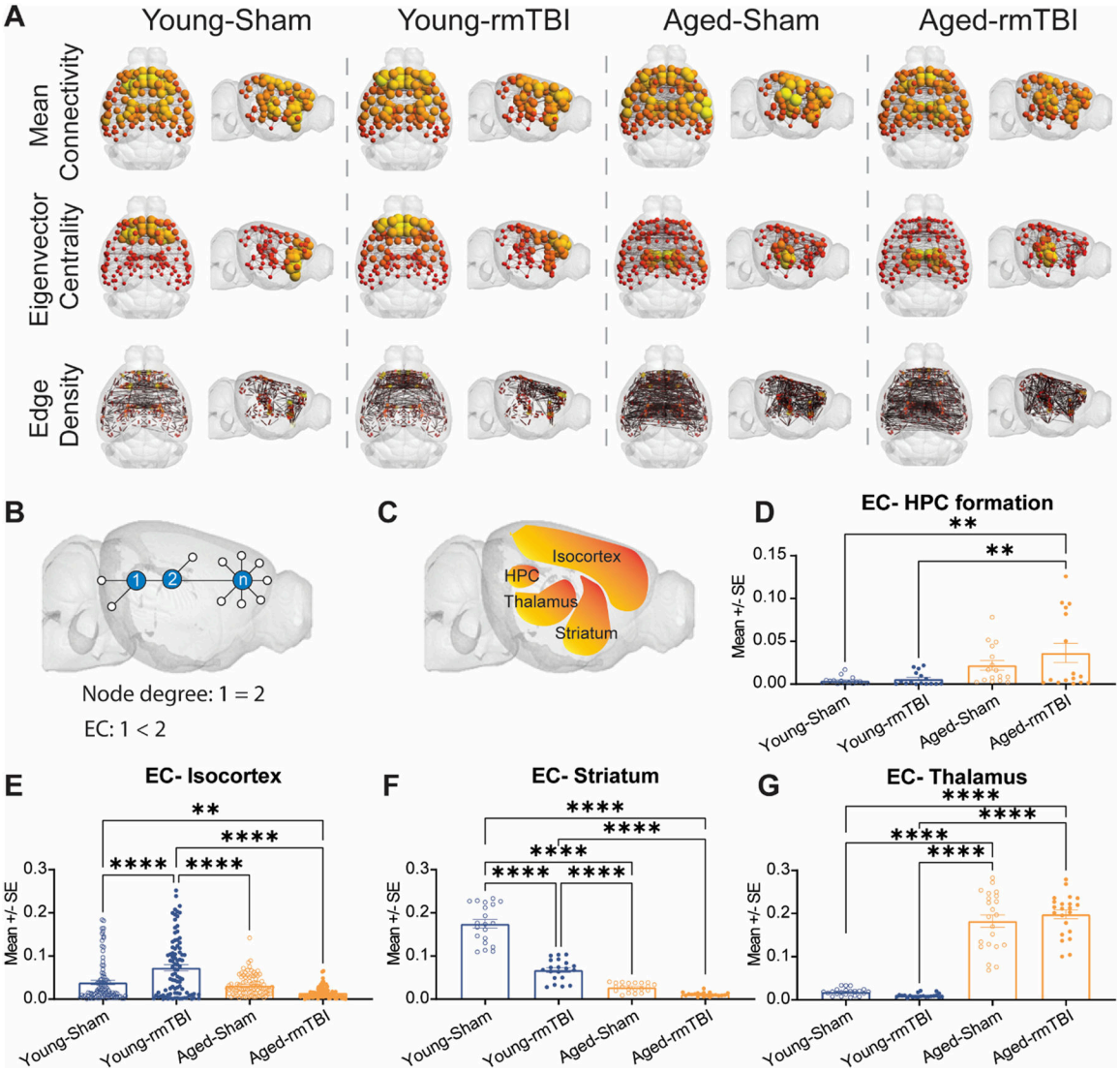

Fig. 5.

Functional brain connectivity by subdivisions. (A) Connectome maps illustrating the average functional connectivity, eigenvector centrality, and total edge densities among all ROIs within the groups. (B) A basic diagram depicting node degree and eigenvector centrality relationship. (C) Brain areas were further dissected into subdivisions showing age differences in eigenvector centrality in the (D) hippocampal formation, (E) isocortex, (F) striatum, and (G) thalamus. Statistically significant *p*-values from two-way ANOVA are represented as follows: ** $p < 0.01$, **** $p < 0.0001$. EC = eigenvector centrality, HPC, hippocampus; ROI, regions of interest.

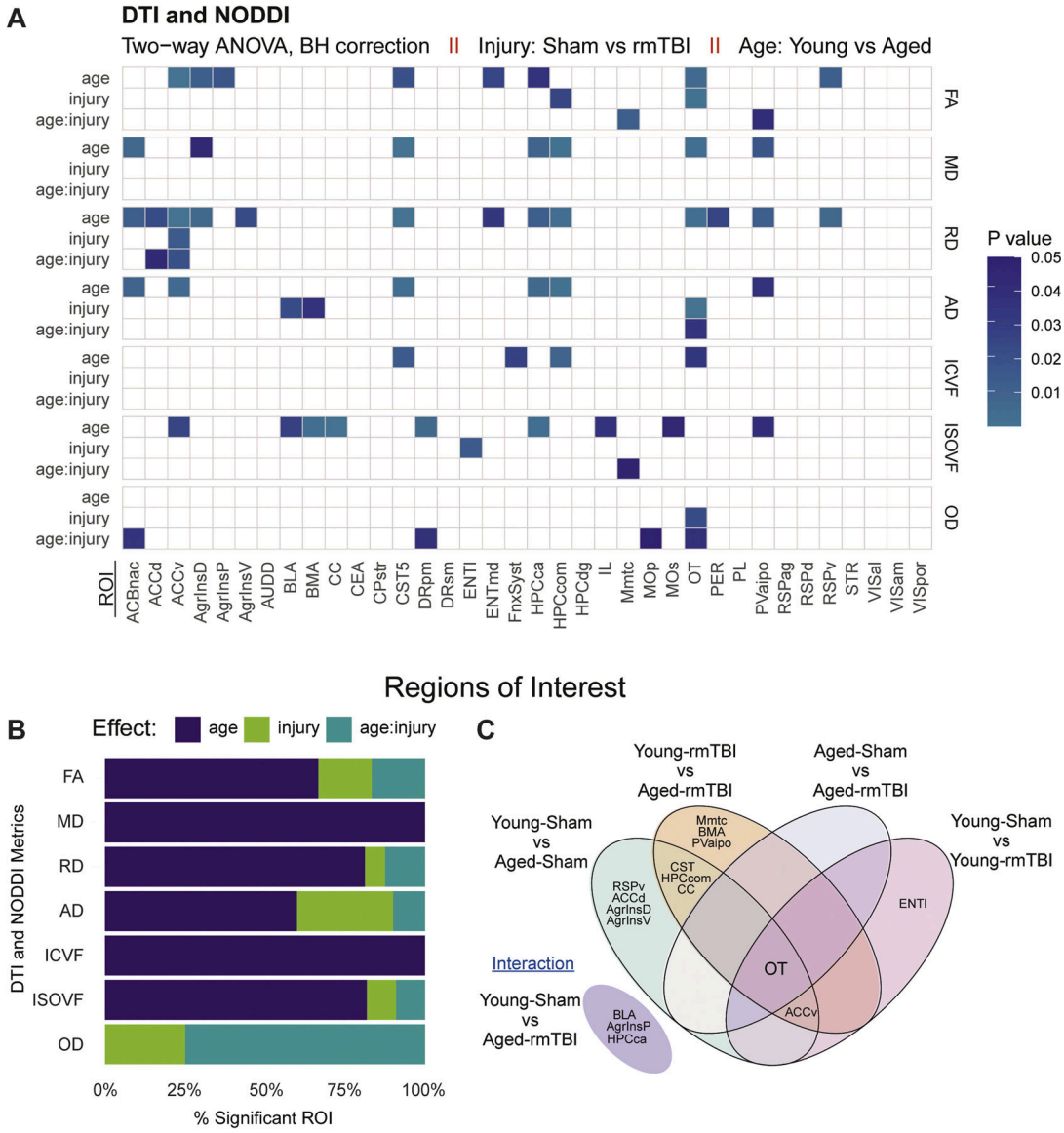

Fig. 6.

Microstructural changes in ROIs: DTI and NODDI metrics. (A) Main effects and interactions on each region of interest (ROI)'s microstructure. Significant adjusted *p*-values resulting from two-way ANOVA (type III) with Benjamini-Hochberg (FDR-BH) correction are color-coded in the heatplot. Diffusion tensor imaging (DTI) metrics include fractional anisotropy (FA, measures directional water diffusion), mean diffusivity (MD, reflects overall water diffusion.), axial diffusivity (AD, measures diffusion along the main voxel axis), and radial diffusivity (RD, analyzes diffusion perpendicular to the main voxel axis). The three compartments measured in neurite orientation dispersion and density imaging (NODDI) analysis were: isotropic volume fraction (ISOVF, quantifies non-neurite components), intracellular volume fraction (ICVF, measures volume taken by neurite), and orientation dispersion index (OD, indicate neurite alignment and organization). (B) The percentage of significant ROIs affected by age (young vs aged), injury (sham vs rmTBI) and interaction

between these factors. (C) Shared regions affected between groups demonstrating the unique effect by age and injury in white matter integrity. Young-Sham (n = 5), Young-rmTBI (n = 4), Aged-Sham (n = 5), and Aged-rmTBI groups (n = 7). Supplemental Table 2 describe ROI names in DTI and NODDI analyses.

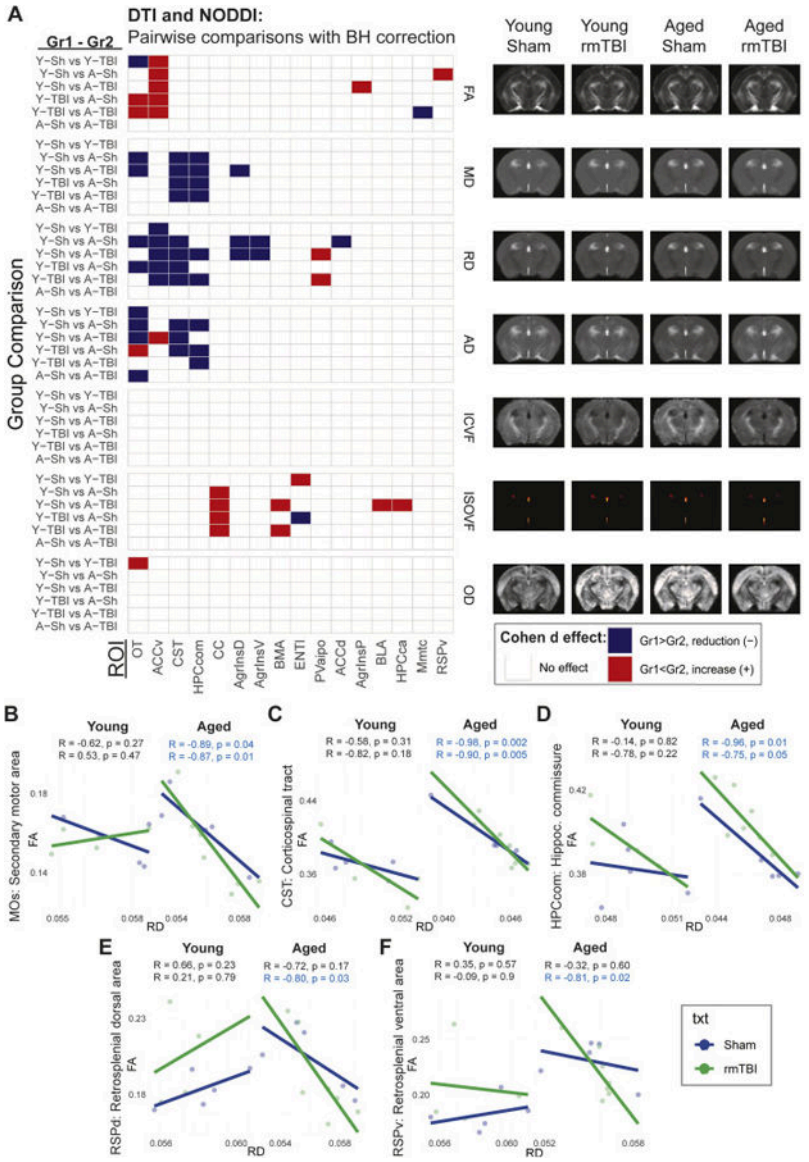

Fig. 7.

Optic tract and anterior cingulate: key regions in DTI and NODDI analysis comparison. (A) Multiple comparison tests were conducted on the regions of interest (ROI) displaying significant main effects in the two-way ANOVA for both DTI and NODDI analyses. DTI measures include fractional anisotropy (FA, directional water diffusion), mean diffusivity (MD, overall water diffusion), axial diffusivity (AD, diffusion along the main voxel axis), and radial diffusivity (RD, diffusion perpendicular to the main voxel axis). NODDI measures comprise isotropic volume fraction (ISOVF, non-neurite components), intracellular volume fraction (ICVF, volume occupied by neurites), and orientation dispersion index (OD, neurite alignment and organization). Significant effects with a large effect size (Cohen's d) are indicated in color, while non-effects are shown in white. Adjusted *p*-values were corrected using Benjamini-Hochberg (FDR) correction. Red signifies an effect size equal to or greater than 0.8, and blue indicates an effect size equal to or less than —0.8. ROIs

are ordered based on the highest number of significant *p*-values, highlighting the optic tract (OT) and anterior cingulate (ACC) as the most affected regions. Representative images correspond to their respective metrics. (B-D) Inverse Pearson correlations between FA and RD for the motor area (MOs), corticospinal tract (CST), and hippocampal commissure (HPComm) indicates an overall reduction of RD by aging. (E-F) Interaction between aging and brain injury augments inverse correlations between FA vs RD signal in retrosplenial area (RSP). Gr1, group1 is first from left to right in panel; Young-Sham (Y-Sh), $n = 7$; Young-rmTBI (Y-TBI), $n = 10$; Aged-Sham (A-Sh), $n = 6$; Aged-rmTBI (A-TBI), $n = 8$.

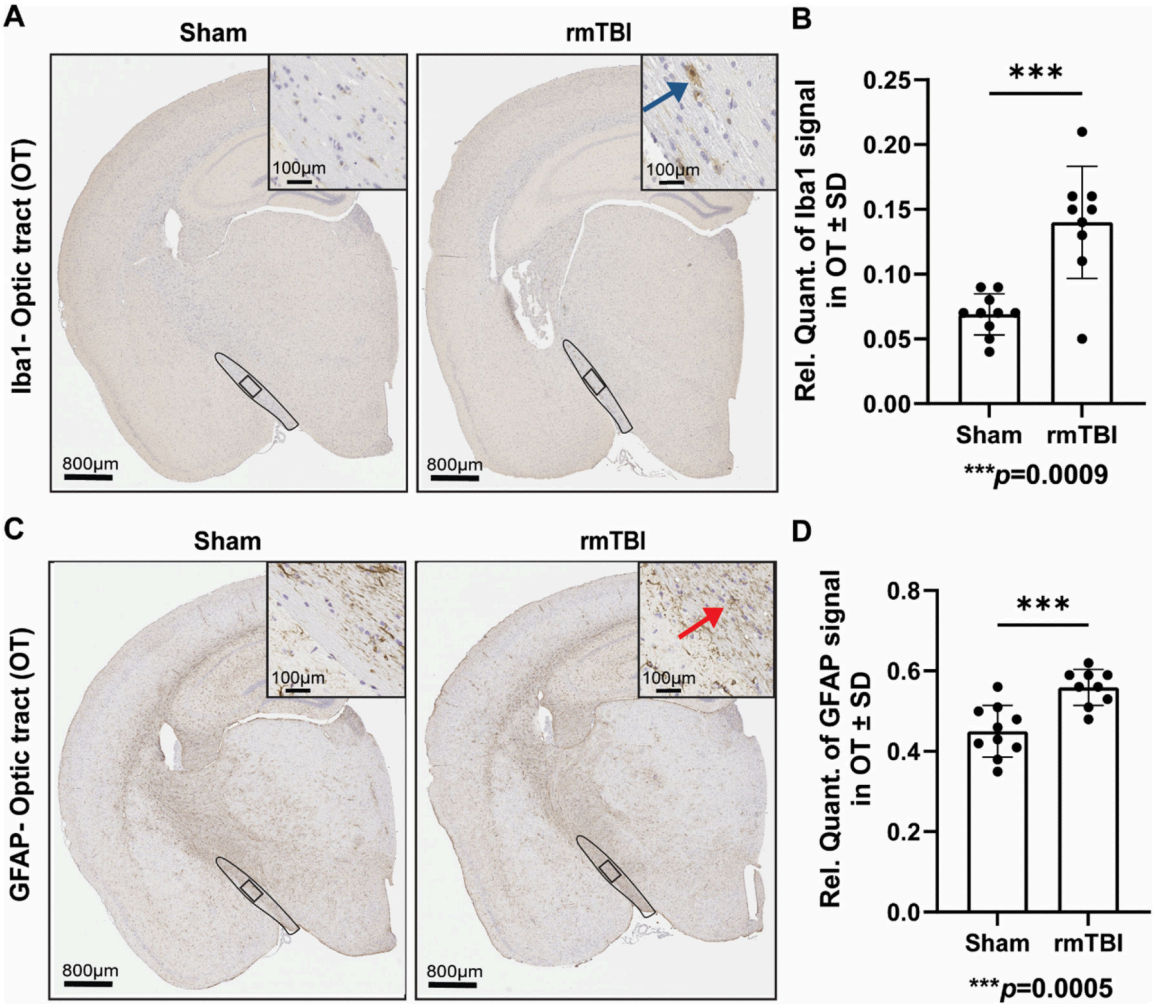

Fig. 8.

Gliosis is induced by rmTBI in optic tract. (A). Following rmTBI, aged mice displayed an increase in (A-B) Iba-1 and (C-D) GFAP expression in the optic tract. Microglia are indicated by the blue arrowhead, and astrocytes by the red arrowhead. Brain coronal view: 800 μm; Scale bar for inset (enlarged view of the optic tract) = 100 μm. Statistical analysis performed using unpaired *t*-test with Welch's correction; Aged-Sham ($n = 10$), Aged-rmTBI ($n = 9$). SD: standard deviation; Iba-1, Ionized calcium-binding adaptor molecule 1; GFAP, Glial fibrillary acidic protein; μm, micrometers; OT, optic tract.